BUDAPEST UNIVERSITY OF TECHNOLOGY AND ECONOMICS
FACULTY OF MECHANICAL ENGINEERING
DEPARTMENT OF POLYMER ENGINEERING

DEVELOPMENT AND INVESTIGATION OF MELT-BLOWN FIBER MATS AND THEIR COMPOSITES

BOOKLET OF PH.D. THESIS

YAHYA KARA
MSC. MECHANICAL ENGINEER

Supervisor:
Dr. Kolos Molnár
Associate Professor

BUDAPEST
2022

Peer reviews of the dissertation and the minute of the defense meeting can be viewed at the Dean's office of the Faculty of Mechanical Engineering of the Budapest University of Technology and Economics

1. Introduction

Generating polymeric fibers is one of the key advancements in polymer engineering and science. In recent years, various techniques such as template synthesis, self-assembly, phase separation, melt blowing and electrospinning developed. Among them, melt blowing is the most feasible technology due to straightforward processing, fair control of fiber morphology, and utilization of a broad range of polymeric materials. In melt blowing, the polymer melt is extruded through a die containing numerous small capillaries and then stretched via a jet of hot air. The higher air velocity versus low velocity polymer jets provides a drag force that rapidly attenuates the polymer jets into fine fibers. Then, the fibers are collected on the surface of a collector in the form of a random web. The lack of controlled stretching gives melt blowing technology a distinct cost advantage and high production rate compared to other micro- and nanofiber mat generating techniques.

The composite laminates made of reinforcing fibers usually exhibit excellent in-plane material properties; however, the matrix material and fiber-matrix interface dominate out-of-plane properties (e.g., interlaminar shear strength). Ply to ply interfaces of composite laminates possess weak areas of the structure due to the nature of the laminates. An interlaminar toughening approach, including incorporating sub-phases into the interface between the reinforcement and the matrix, can effectively solve this issue. The continuous nano- and submicron fibers have a large surface-to-volume ratio and aspect ratio (length/diameter), and they are expected to have better interfacial strength than conventional reinforcing fibers, thus providing advanced interfacial properties. The fine surface morphology and potentially homogeneous dispersion of nano- and submicron fibers throughout the matrix make these fine fibers of great interest in reinforcing composites structures.

Recently, attention has been increasingly devoted to recycling components made of fiber-reinforced polymer composites. That brings new challenges for enhancing these composites' mechanical and thermal characteristics in parallel to their recyclability. This demand led to the development of single-polymer composites (SPCs). SPCs are a particular family of thermoplastic composite materials in which both the reinforcing fiber and the polymer matrix are from the same polymer family. They can be easily recycled by melting both (similar) components. However, their production requires complex techniques (*e.g.*, film-stacking, hot compaction, coextrusion) and sensitive processing parameter control to prevent the reinforcing fibers from being completely melted. Although the SPCs are not new, difficulties in processing and limited load-bearing ability and thermal performance still hamper SPCs' applicability in industrial utilization. In this regard, melt-blown (MB) fiber mats with a large surface-to-volume ratio can establish excellent interfacial strength, and therefore they might enhance SPCs' performance.

MB fibers and related products are used in many applications, including but not limited to automotive, railway, aerospace, agriculture, geotextiles, industrial/military, medical/healthcare and construction. The demand for personal protective equipment (PPE) made of MB fibers has soared to unprecedented levels due to the COVID-19 pandemic. Reports indicate that only in 2020, over 50 billion face masks made of nonwovens were produced, while it is estimated that 1.6 billion of these masks ended up in oceans. The automotive nonwoven market worldwide rated around 10 billion USD in 2018, while it is expected to extend to 14.2 billion USD by 2026. Yet, most nonwovens are not entirely environmentally friendly since they are made of non-biodegradable polymers. Therefore, demand for recyclable and sustainable fine fibers, such as biopolymer fibers is rapidly

emerging. Limited attention has been devoted to the degradation and decomposition of biopolymer-based nano- and microfibrous structures.

In this regard, I investigated controlling and modifying MB polymeric fibers' performance by controlling processing parameters. I proposed a novel approach for making high-performance SPC with MB fine fiber interleaves. Furthermore, I developed nanocomposite MB fibers to enhance SPC laminate stiffness and damage tolerance. Besides, I generated high-performance poly (lactic acid) (PLA) MB fibers and conducted a systematic and comparative analysis of PLA fine fibers' hydrolytic and composting behavior. Finally, I discovered a new method of making nano-/submicron fibers via fused filament fabrication (FFF) technology. I designed a novel apparatus capable of generating continuous fine fibers and printing 3D structures to create hierarchical structures.

2. Summary of the literature overview, goals

An overview of various investigations on melt blowing, MB fibers and related fiber-reinforced polymer composites have been presented. It is realized that the MB fiber properties and fiber mat performance are very sensitive to processing parameters. Up to date, both industry and academy put considerable effort into the development of the MB fiber mats for various applications. There are still many challenges for further optimization, end-product designing, characterization, and process modeling in practice despite the advances in the development of MB fiber mats. Even though many researchers have dealt with melt-blowing and related process dynamics, there is a lack of knowledge that analyzes fiber formation mechanisms, crystalline structure, thermal and structural behavior of MB fiber mats, molecular structure development and thermal behavior accordingly.

Current attention is devoted to the sustainability and recyclability of composite structures besides advancing their thermal and mechanical properties. These concerns in the composite research led to the development of SPCs. Although such structures are not new, difficulties in processing and limited load-bearing ability and thermal performance still hamper their applicability in industrial utilization. Incorporating nano- and submicron fiber interleaves can be feasible since only a small amount of such fine fibers may be sufficient to achieve high performance.

The MB fibers performance of synthetic nano/submicron fibers might be enhanced by nanoparticle inclusion. One might expect that the nanoparticles embedded within the fibers may boost the modulus and strength of these fibers. However, achieving uniform dispersion of the nano inclusion in a polymer matrix is challenging, and poor dispersion can deteriorate properties. In this regard, developing fine fiber and composite manufacturing methods is demanded for future engineering applications.

Many efforts have been made to unfold the biodegradation and decomposition of biopolymers and their derivatives, mainly for films or injection molded products. The main idea behind these efforts is to show carbon dioxide neutrality through biodegradation after their service life, solving the polymer waste disposal problem. Demands for lightweight, durable, porous, self-bonded and biodegradable technical nonwovens are unprecedentedly increased nowadays, yet their decomposition characteristics in water and compost are not unveiled. Even though many researchers have dealt with the degradation of biopolymer products, up to date, limited attention is devoted to the degradation and decomposition of biopolymer-based nano- and microfibrous structures.

Recent polymer engineering and technology advancements provide potent tools for fabrication products and devices with complex geometries. Up to date, fiber spinning techniques and AM methods are expanded only with robotic control in the corresponding

machine assembly for generating fibers. However, it remains unexposed to generate continuous thin fibers and integrate them with 3D printed structures via the FFF method. Although the precision of recent 3D printers and the quality of 3D printed objects have gradually improved so far, the 3D printing of fine fibers and related hierarchical structures with a single FFF apparatus remains a great challenge.

Based on the literature overview, the objectives of this thesis are listed as follows:

- To understand the relationship between melt blowing parameters and fiber morphology, fiber formation mechanisms, crystalline structure, thermal and structural properties.
- To develop MB fiber mat reinforced SPCs and investigate the effect of fine fibers on the composite's thermal and mechanical properties.
- To develop a method for producing high-performance SPCs with MB fiber mat interleaving veils without compromising recyclability, lightweight and straightforward processability.
- To develop nanoparticle-doped MB fibers with enhanced thermal and mechanical properties and apply them as interleaving veils for producing high-strength SPCs.
- To develop biopolymer-based MB fine fiber mats and test their decomposition characteristics in water and composting soil.
- To develop a new method of making synthetic fibers and hierarchical structures via FFF technology for advanced engineering applications and demonstrate its feasibility for controlling fiber properties.

3. Materials, machines, and test methods

This chapter introduces the materials and the equipment and test methods used for the characterization of the melt-blown fiber and polymer composites samples.

3.1. Materials

Borealis HL712FB type homopolymer polypropylene (PP) was used for the preparation of fiber mats and a compression molded sheet was used as reference.

I prepared fiber mats using Borealis HL512FB type PP homopolymer for producing hot compacted single-polymer composites.

HL912FB type PP homopolymer was used to prepare fine fiber mats for producing an interleaving veil. A plain-woven PP fabric was used to produce single-polymer composites. I used a low modulus isostatic PP (LiPP) and a random copolymer PP (rPP) (RJ470MO) for producing matrix films.

HL912FB type PP homopolymer and LiPP were blended in a mass ratio of 9:1 for the preparation of fine fiber mats via melt blowing. A commercially available multiwalled carbon nanotube (MWCNT) Nanocyl™ NC7000 (Nanocyl S.A., Belgium) material was used to prepare MWCNT-doped PP fibers. I also used LiPP and an R1059A rPP for making a matrix film.

PDLA homopolymer and PLLA homopolymer resins were used for the preparation of fine fiber mats for investigating decomposition characteristics in compost and in water.

PLLA homopolymer resin was used to prepare filaments for FFF 3D printing.

3.2. Melt blowing setup used

For the melt-blowing experiments, a custom laboratory unit was built. A custom dual-slot melt blowing die and was mounted to a LE8-24C type single-screw laboratory extruder

(LabTech, Thailand). The extruder had a single screw with 8 mm diameter and 24 L/D ratio screws. The die had 40 fiber-forming capillaries, 330 μm diameter each, arranged in a single row. The temperatures of the four (2 in parallel-2 in serial) inline heaters were measured in line with two, K-type, inline nozzle thermocouples. The hot air temperature was controlled by a PID controlling unit. Besides the air heating, the die itself was heated by cartridge heaters. An RTD Pt100 sensor and a PID control unit were used to heat up and control the temperature of the die. The collector was a drum with a diameter of 200 mm.

3.3. Extruders and auxiliary equipment used

I used a twin-screw (counter-rotating) extruder (Labtech LE 25–30/C, Thailand) for compounding PP and PLA resins. The extruder was equipped with 26 mm diameter, 44 L/D screws. The extruder was equipped with a double-orifice extruder die. I used an LZ-120/VS granulator (Labtech, Thailand) to chop filaments into 1-3 mm pellets.

I used an LF-400 type laboratory extruder followed by a small sheet film line (LabTech LCR300, Thailand) for producing thin films. This extruder has a single 25 mm diameter, 30 L/D screw. The extruder was equipped with a 200 mm wide coat hanger type die.

3.4. The hot press used to produce single-polypropylene composites

I used a Polystat 300S type hydraulic hot press (Maschinenfabrik Fr. Schwabenthan & Gomann, Germany). The hot press platen size was 300 x 300 mm. The hot press temperature was controlled by PID controlling units with a measuring accuracy of ± 2°C. The cooling system consisted of circulating water in the upper and lower platens.

3.5. Manufacturing fine polypropylene fiber mats for revealing the process–structure-property relationships

The die and extruder temperatures were kept constant and set to 225 °C. The hot air temperature was set between 125 to 300 °C. Various air pressures were set in the range of 1-2.5 bar. The circumferential velocity of the drum collector was calculated and varied between 12-105 m/min. The extruder screw speed was set constant at 1 rpm. The variable DCD (50-500 mm) was used. The sample processing time was 10 min.

I produced sheets of HL712FB type hPP to analyze its molecular structure with MB fibers produced with the same polymer. 50 g of hPP was melted in a 55 cm^3 Brabender internal mixer (Brabender Plasti-Corder, Brabender GmbH & Co. KG, Duisburg, Germany) equipped with counter-rotating mixing elements, operating at 50 rpm for 10 min at 200 °C. The resulting material was subsequently hot-pressed in a laboratory press (Teach-Line Platen Press 200E, Dr. Collin GmbH, Munich, Germany) at 225 °C for 10 min under a pressure of 2.8 MPa applied on square plates of 140 × 140 mm. With the method used, I obtained a 0.8 mm thick h-PP sheet.

3.6. Manufacturing hot-compacted single-polypropylene composites made of melt-blown fiber mats

I prepared fiber mats using Borealis HL512FB type hPP for generating hot compacted single-PP composites. The die and extruder temperatures were constant and set to 250 °C. The temperature of the pressurized air (1.4 bar) was set to 200 °C. The DCD was set to 150 mm. A drum with a diameter of 160 mm and rotation speed of 60 rpm was used as the collector and the sample processing time was 10 min.

I produced single-PP composites by hot compaction with a hot press. I laid one nonwoven strip in a U-shaped metal mold. The length and width of the mold were 300 mm and 15 mm, respectively. The samples were compression molded for 15 s with a compression pressure of 3 MPa (on the sample). One set of the samples was cold-pressed (in this case, the room temperature was 28.8 °C), then I made samples with hot compaction at three different

temperatures: 125, 135 and 145 °C. The thickness of the hot compacted samples was around 0.69±0.14 mm.

3.7. Manufacturing hierarchical single-polypropylene composites interleaved with melt-blown polypropylene fiber mats

I produced a PP blend made of 10 wt% LiPP and 90 wt% rPP (RJ470MO) with a twin-screw extruder. The extrusion temperature was set to 170°C-170°C-180°C-180°C-185°C-185°C-190°C-190°C-200°C-200°C (from hopper to die). Feeder speed and screw rotation speed were set at 10 rpm and 40 rpm, respectively.

Thin films of the PP blend were prepared with an LF-400 type laboratory extruder followed by a small sheet film line. The extruder screw rotation speed was set to 50 rpm. The extrusion temperature was set 180°C-185°C-190°C-195°C-200°C (from hopper to die). The die slit distance was set at 0.5 mm. The flat film take-up cylinder (Ø145) temperature and pulling speed were set to 70 °C and 10 rpm, respectively. The speeds of the lower (Ø72.5) and upper (Ø72.5) take-off rolls were 2 and 2.8 rpm, respectively. The thickness of the film produced was 70 ± 5 μm.

I produced fiber mats using HL912FB hPP for preparing an interleaving veil for making a single-PP composite. The die and extruder temperatures were set to 225 °C. The air temperature and pressure were set at 275 °C and 2.5 bar, respectively. The extruder screw speed was set at 1 rpm. Collector drum circumferential velocity was set at 28 m/min. The DCD was set to 400 mm. The collector drum was covered with the woven PP fabric, and MB fiber mats were collected directly onto those.

The blend film (F) was used as a matrix, while woven fabric (W) was the reinforcement for the single-PP composite sheets. It was compared with the composites that are interleaved with the MB fiber mat (F/MB/W). The composite stack consisted of 6 layers of film (F) and 5 layers of woven fabric (W), while those composites interleaved with MB fiber mat (MB) had 4 layers of fiber mat distributed in between the film and the woven fabric. I also made a W/MB sample without any film. The composite sheets were produced by film-stacking with a Polystat 300S hydraulic hot press. The layered stack was placed into this mold and then put into the hot press set at the designated molding temperature (*i.e.*, 150, 155, 160 °C). After closing the mold, it was kept for 30 s without pressure to equilibrate the temperature. Then the compression molding pressure was set at 5 MPa (actual pressure on the specimen) while the holding time was fixed at 120 s. SPC sheets had a thickness of 1.9 ± 0.1 mm. The layer order of the composites is illustrated in Figure 1.

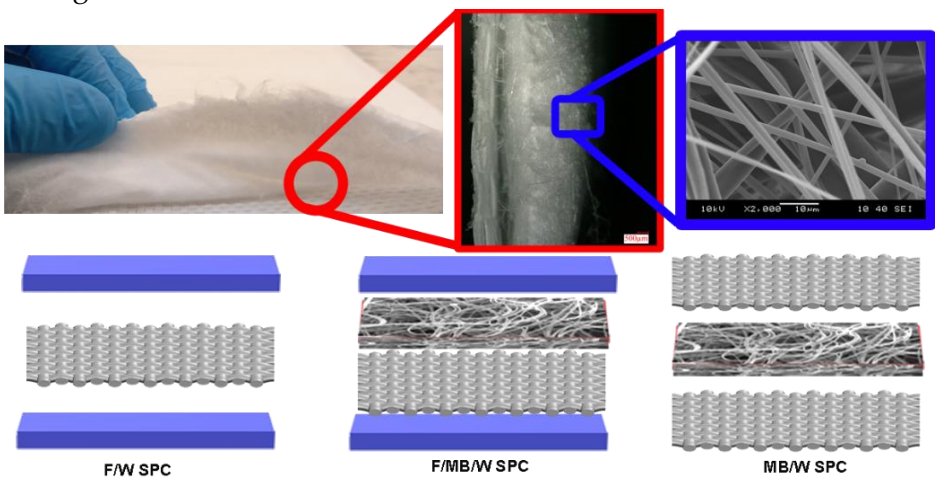

Figure 1. Demonstration of the MB fiber mat and woven fabric interface and the representative single-PP composite stacking sequence

3.8. Manufacturing single-polypropylene composite interleaved with MWCNT doped polypropylene fine fiber mat

A PP/MWCNT nanocomposite masterbatch was produced with an MWCNT concentration of 5 wt% and with 47.5 wt% LiPP and 47.5 wt% hPP. After that, I diluted the masterbatch to MWCNT concentrations of 0.05, 0.1, 0.25, 0.5 and 0.75 wt% with LiPP and hPP in a mass ratio of 1:9. A PP blend was also prepared with a composition of 10 wt% LiPP and 90 wt% hPP for generating reference PP MB fibers.

I used a twin-screw extruder, and the extrusion temperature was set to 160°C-160°C-160°C-170°C-170°C-170°C-180°C-180°C-190°C-190°C (from hopper to die). Feeder speed and screw rotation speed were set at 7.5 rpm and 30 rpm, respectively.

For PP matrix film, a PP blend made of 10 wt% LiPP and 90 wt% rPP (R1059A) was produced with a twin-screw extruder. The extrusion temperature was set to 170°C-170°C-180°C-180°C-190°C-190°C-195°C-195°C-200°C-200°C (from hopper to die). Feeder speed and screw rotation speed were set at 15 rpm and 60 rpm, respectively.

I prepared the PP blend thin films to use as a matrix in SPCs manufactured by film-stacking. I used the extruder and flat film line introduced in Chapter 3.3. The slit distance was set at 0.4 mm. The speeds of the lower (Ø72.5 mm) and upper (Ø72.5 mm) take-off rolls were 4 and 3.4 rpm, respectively. The screw rotation speed was set to 40 rpm. The extrusion temperature was set 180°C-185°C-190°C-195°C-200°C (from hopper to die). The flat film take-up cylinder (Ø145 mm) temperature and pulling speed were set to 70 °C and 20 rpm, respectively. The thickness of the film produced was 60 ± 5 μm.

I produced MWCNT-doped PP fiber mats (0, 0.05, 0.1, 0.25, 0.5 and 0.75 wt%) to investigate the MWCNT effect on fiber mat morphology, thermal and mechanical properties. The die and extruder temperatures were set to 250 °C. The air temperature and air pressure were set at 285 °C and 2 bar, respectively. The extruder screw speed was set at 5 rpm. The DCD was set to 300 mm. The drum's circumferential velocity was set at 28 m/min. The sample processing time was 5 min.

I used an 0.1 wt% MWCNT doped PP MB fiber mat (nanoPPMB). The blend film (F) was used as a matrix, while woven fabric (W) was the reinforcement for single-PP composite laminates. The reference SPC (F/W) stack consisted of 7 layers of PP film (F) and 6 layers of woven fabric (W), while those SPCs interleaved with PPMB (F/PPMB/W) and nanoPPMB (F/nanoPPMB/W) fiber mats had 5 layers of fiber mat distributed in between the film and the woven fabric.

I used the same hydraulic press, mold and settings for producing composites explained in Chapter 3.7. The layered stack was placed into this mold and then put into the hot press set at 154 °C (FFFF). The thickness of the SPC sheets was 2.35±0.1 mm. The SPC lamina stacking and the compression molding process are illustrated in Figure 2.

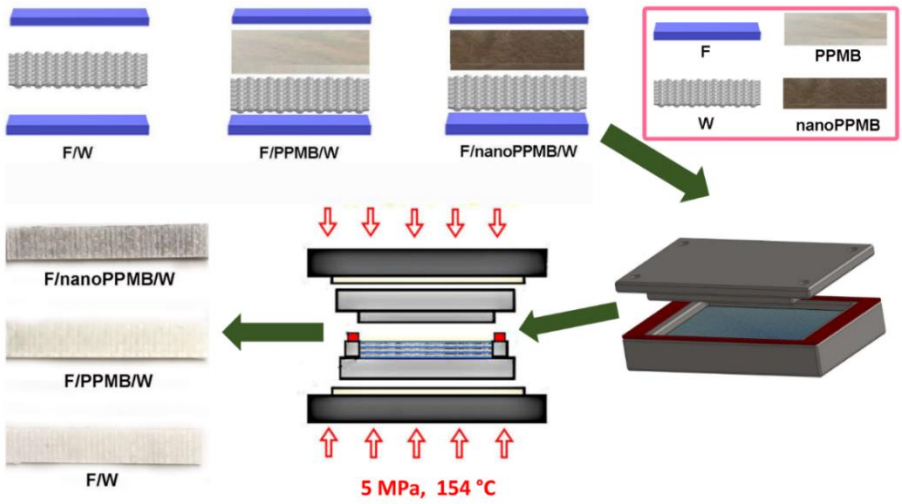

Figure 2. Schematic diagram of the SPC production process

3.9. Manufacturing Stereocomplex poly (lactic acid) fiber mats

I produced a stereocomplex PLA via melt stereocomplexation using L and D enantiomers. I mixed PLLA and PDLA in a weight ratio of 0:1 (PLLA), 3:1 (3D1L), 1:1 (1D1L), 1:3 (1D3L), and 1:0 (PDLA) by dry mixing. I used a twin-screw extruder and the extrusion temperature was set to 220°C-220°C-225°C-225°C-225°C-230°C-230°C-235°C-235°C (from hopper to die). Feeder speed and screw rotation speed were set at 15 rpm and 60 rpm, respectively.

I generated various stereocomplex and homocrystalline PLA MB fibers to test their decomposition characteristics in water and soil compost. The die and extruder temperatures were set to 240 °C. The air temperature and pressure were set at 250 °C and 2 bar, respectively. The extruder screw speed was set at 1 rpm. The DCD was set to 200 mm. The drum's circumferential velocity was set at 28 m/min. The sample collection time was 10 min for all the compositions.

4. Characterization methods

The characterization techniques include scanning electron microscopy (SEM), fiber orientation measurement, density, porosity and pore size measurement, wide-angle X-ray diffraction (WAXD), differential scanning calorimetry (DSC) and thermogravimetric analysis (TGA) and capillary rheometry. I performed dynamic mechanical analysis (DMA), tensile, short beam shear (SBS) and instrumented falling weight impact (IFWI) tests to evaluate the mechanical properties of fiber mats and composite samples. In addition, I conducted composting tests according to the ISO-20200 standard for PLA MB fiber mats to characterize their decomposition behavior in soil. I also evaluated PLA MB fiber mat's hydrolytic decomposition characteristics in water. I employed computational fluid dynamics (CFD) simulations to characterize the airflow field of the developed apparatus.

4.1. Scanning electron microscopy (SEM)

The morphology of fiber and composite samples was observed using scanning electron microscopy (SEM; JEOL 6380 LA, Japan). I pasted samples onto metallic studs with double-sided conductive tape. The surface of the fiber mat and composite samples were finely coated using a JEOL JFC-1200 (Jeol Ltd., Japan) fine coater with gold (Au) in order to avoid their charging. I measured 100 fibers for each sample to analyze the melt-blown fiber diameter and pore size distributions. I used ImageJ 1.51k (WS Rasband, National Institutes of Health, USA,) software for this measurement.

4.2. Characterization of fiber mat physical properties: fiber orientation measurement, density, porosity and pore size measurement

The bulk density of each fiber mat was determined by measuring the mass and taking the dimensions with digital calipers (Fowler Promax, USA). Samples were cut to 40x20 mm rectangles. The fiber mat thicknesses were measured using a micrometer (Louis Schopper Leipzig, Germany) with a precision of 0.01 mm. The density of the raw polymer was determined based on the Archimedes principle in methanol (Vegyszer Kereskedelmi Kft., Hungary) at 23 °C according to EN ISO 1183-1 by using a Sartorius Quintix 125D-1CEU (Sartorius, Germany) semi-micro scale. Porosity (*P*) and solidity (*S)* of the nonwovens were determined by using Equations 1-3.

$$\rho_{f,m} = \frac{m_{f,m}}{v_{f,m}} \; [g/cm^3] \tag{1}$$

$$P = \left(1 - \frac{\rho_{f,m}}{\rho_{polymer}}\right) x \; 100 \; [\%] \tag{2}$$

$$S = (1 - P) \; x \; 100 [\%] \tag{3}$$

where, $\rho_{f,m}$ is the fiber mat bulk density, $m_{f,m}$is the fiber mat mass, $v_{f,m}$is the volume of the fiber mat, $\rho_{Polymer}$ is the bulk polymer density, ρ_a is the areal density, $t_{f,m}$ is the fiber mat thickness.

The PP MB fiber mats' pore size was determined using image analysis. I tested five samples for each group. Five different images were captured for each fiber mat sample. I considered 500 pores for each sample to analyze the MB fiber mat average pore size distributions. The feret diameters were automatically measured from the SEM images taken for each fiber mat using ImageJ 1.51k software.

4.3. Characterization by wide-angle X-ray diffraction (WAXD)

The crystal structure of the PP fiber and compressed PP sheet samples was investigated by X-ray line profile analysis. The XRD patterns were measured by an RA-MultiMax9 (Rigaku, Japan) rotating anode diffractometer using CuKα1 radiation with a wavelength of λ = 0.15406 nm. I analyzed the distance between the lattice planes and the corresponding Miller indices [hkl] of the main Bragg reflections relative to the α, β, γ and mesomorphic forms of isotactic PP according to the literature data. The related analysis method by the Scherrer and Bragg equations. I analyzed the crystallite size (L) of a given reflection by using the Scherrer equation (Equation 4) while the distance between lattice planes (d) was calculated by Bragg's law (Equation 5)

$$L = \frac{K \lambda}{\beta \cos \theta} \tag{4}$$

$$d = \frac{\lambda}{2 \sin \theta} \tag{5}$$

where K is the Scherrer constant (0.89), λ is the X-ray wavelength, θ is the diffraction angle of the [hkl] reflection and β is the full width at half max (FWHM).

4.4. Characterization by differential scanning calorimetry (DSC) and thermogravimetric analysis (TGA)

The thermal properties of the polymer granules (e.g., pristine blends), the MB fibers, the films and the composites were studied by differential scanning calorimetry (DSC) with a Q2000 DSC (TA Instruments, USA) device. The tests were performed in an inert atmosphere (N2; 50 ml/min purge flow rate) at a temperature range of -50 to 220 °C for PP with a heating and cooling rate (heat ramp) of 10 °C/min, while the temperature range was 0 to 250 °C for PLA with a heating and cooling rate (heat ramp) of 5 °C/min. The degree of crystallinity (χ) of the fibers was determined based on Equation 8. 207 J/g, 97 J/g and 147 J/g were considered for

the heat of fusion of the 100% crystalline (ΔH_m^0), h-PP, homocrystal PLA and stereocomplex PLA, respectively, in the analysis (Equation 6):

$$\chi = \frac{\Delta H_m - \Delta H_{cc}}{\Delta H_m^0} \times 100\ [\%] \quad (6)$$

where, ΔH_m is the experimental heat of fusion and ΔH_{cc} is the experimental cold crystallization obtained by the DSC scans.

To characterize the fibers and composite's thermal characteristics, TGA was performed using a TA Instruments (USA) thermogravimetric analyzer TGA Q500 between 50 °C and 600 °C at a heating rate of 10 °C/min under nitrogen purge flow (60 ml/min).

4.5. Rheology tests

The shear viscosity of the pristine (0 wt%) and MWCNT doped (0.1, 0.25, 0.5 and 0.75 wt%) PP resins were measured with a capillary rheometer (Instron 13 Ceast SR20). The testing temperature was set to 180 °C. I measured the shear viscosity in the 100-7,500 1/s shear rate range, using a capillary with a length and diameter of 20 mm and 1 mm, respectively.

4.6. Characterization of mechanical properties

4.6.1. Tensile tests of fiber mat tests and hot-compacted PP SPCs

I prepared rectangular samples in 40 mm x 10 mm for MB fiber mat tensile tests. The tensile properties of the fiber mats were tested at room temperature with a Zwick Z005 (Zwick, Germany) type universal tensile tester equipped with a 20 N load cell. The gauge length was set to 20 mm. The testing routine was performed 5 times for each sample group. The tensile speed of 10 mm/min was applied. I calculated the area by using Equation 7.

$$A = \frac{\mathrm{m}_{fm}}{l_{fm}\rho_{Polymer}} \quad (7)$$

where, m_{fm} is the fiber mat mass, $l_{fm}$is the length of the fiber mat and $\rho_{Polymer}$ is the polymer bulk density (PP =0.889 g/cm^3, PLA=1.24 g/cm^3).

4.6.2. Hierarchical single-PP composites interleaved with MB PP fiber mats tensile tests

The blended PP matrix film and the composite samples were cut to 150 x 20 mm rectangles. The SPC samples were tensile tested at room temperature to 5 mm/min with a Zwick Z020 (Zwick, Germany) machine equipped with a 20 kN load cell. The gauge length was set at 90 mm. The testing routine was performed 7 times for each sample group. The tensile strength, elastic modulus and secant modulus at 0.5%, 1%, 2%, 10% strain were evaluated together with their standard deviation.

4.6.3. PP/MWCNT fine fiber mat interleaved SPC tensile tests

The SPCs tensile test was conducted using a Zwick Z250 (Zwick, Germany) test rig with a maximum 250 kN load capability. Samples were cut in 150 mm x 20 mm (length x width). The test speed and gauge length were set at 5 mm/minute and 90 mm, respectively. A full-field strain measurement was done with a digital image correlation (DIC) method using a Mercury Monet (Sobriety Sro., Kurim, Czech Republic) device. A strain analysis software from Mercury RT-v2.6 was used for local strain measurement. I examined 7 samples for each group and analyzed the tensile modulus, the tensile strength, and the strain at break

4.7. Short beam shear (SBS) tests

I conducted short beam shearing (SBS) tests to determine the SPC sample's interlaminar shear strength at room temperature based on the ISO 14130 standard. I cut the composite sheet into 20 x 10 mm specimens. A Zwick Z020 type universal tensile tester with 20 kN load cell at 1 mm/min test speed was used. The test setup was equipped with a 3-point bending fixture,

and the span length was set to 10 mm. 5 samples were tested for each group. The interlaminar shear strength (τ_{ILSS}) was determined by using Equation 8.

$$\tau_{\mathrm{ILSS}} = 0.75 \times \frac{F_{max}}{bt} \quad (8)$$

where, F_{max} is the maximum load observed during and the test, b is the width of the specimen and t is the thickness of the specimen.

4.8. Instrumented falling weight impact (IFWI) test

I investigated the impact properties of the SPC sheets with an instrumented falling weight impact (IFWI) tester (CEAST 9350. Instron, USA). For this, 70 x 70 mm square specimens were cut. The total mass of the dart was 28.41 kg, the dart diameter (hemispherical) was 20 mm, the diameter of the supporting ring was 40 mm, the falling height was 1 m, and the impact energy was 299.1 J. I tested 7 samples for each group at room temperature. The perforation energy (total absorbed energy/specimen thickness) was calculated to characterize the SPC sample's impact behavior. The ductility index was determined as the ratio of the total impact energy to the energy absorbed until the maximum load.

4.9. Dynamic mechanical analysis (DMA)

I conducted dynamic mechanical analysis (DMA) frequency sweep tests in three-point bending mode under a strain-controlled program with a Q800 (TA Instruments, USA) device. I cut 60 x 10 mm (length x width) specimens for this. The small-amplitude frequency-sweep experiments were performed between 1–100 Hz (5 points per decade) at different temperatures ranging from 30 to 110 °C (10 °C increments). The strain amplitude and the heating rate were 20 μm and 3 °C/min, respectively. The results obtained were used to draw the van Gurp–Palmen (vGP) plots and to generate master curves using the time-temperature superposition (TTS) principle. The curves obtained at the various temperatures were shifted horizontally using the Williams-Landel-Ferry (WLF) equation (Equation 9).

$$\log a_t = \frac{-C_1(T-T_{ref})}{C_2+(T-T_{ref})} \quad (9)$$

where C_1 [-] and C_2 [K] are constants, a_t is the shift factor, T_{ref} is the reference temperature [K], T is the arbitrary temperature [K].

One-tailed t-tests (Equation 10) were performed using interleaved and non-interleaved SPCs samples in order to evaluate the effect of the MB fiber mat interleaving on the impact performance of the SPCs. The p values less than 0.05 (level of significance) were considered significantly different.

$$t = \frac{\bar{x}+\mu}{\frac{SD^2}{\sqrt{n}}} \quad (10)$$

where, $\bar{x}$ is the mean of the sample, μ is the assumed mean, SD is the standard deviation and n is the number of observations.

4.10. Poly (lactic acid) fiber mat decomposition study

I conducted composting tests for PLA MB fiber mats to characterize their decomposition behavior in soil. Composting conditions were set and ensured according to the ISO-20200 standard. Fiber mats were cut (30 x 30 mm2) and buried a few cm deep in plastic reactors containing the compost medium. Reactors were then introduced in a climate chamber (Climacell 111, MMM Group, Germany) at 58 °C. Fibers were recovered from the disintegration container at different times (7, 14, 21, 28 and 35 days) and dried in a vacuum drying chamber (VD 53, Binder GmbH, Germany) at 30 °C under vacuum (1 bar) for 72 hours prior to analytical tests. Composting and disintegration were photographed for all samples periodically.

I conducted hydrolytic decomposition tests for PLA MB fiber mats to characterize their decomposition characteristics in water. PLA MB fiber mats' hydrolytic degradation tests were conducted in bidistilled water at 58 °C. Since this temperature was given for composting and disintegration tests according to the ISO standard, I also adopted this temperature for the hydrolytic degradation studies. Several rectangular pieces of fiber mats of each sample type were placed in glass vessels containing bidistilled water. The mass amount of water was fixed in the ratio 500:1 with the mass of the fiber mat sample. In the first 4 weeks, each vessel was emptied using a fine filter paper every week. From the 5th week, each vessel was emptied fortnightly until the 10th week. Fresh bidistilled water was then added to the vessel containing the sample, and the vessel was put again in water at 58 °C. The bidistilled water amount was kept the same. The samples were removed from the hydrolytic medium: one sample per week from week 0 to 4 and one sample fortnightly between week 4 and 10. The extracted samples were dried in a drying chamber (VD 53, Binder GmbH, Germany) at 30 °C under a vacuum (1 bar) for 72 hours prior to DSC and TGA tests.

4.10. Fused filament fabrication (FFF) experiments

I invented a new approach and a FFF apparatus that generates continuous nano-/micro fibers and fabricates hierarchical structures via FFF technology. The novel apparatus combines FFF printing and the continuous nano-/micro fibers generating simultaneously. The ultrafine fibers were generated with the aid of hot pressurized airflow. An exploded view of the apparatus is shown in Figure 3. The opening between the heated block (8) and the air knife (7) can be adjusted by tightening and loosening bolts (10, 11). The opening between the heated block and air knife allows the nozzle in and out from the air knife module (Figure 20). A heat-resistant O-ring (9) avoids air leakage during the operation. When the nozzle is inside the air knife, the apparatus works in the continuous fine fiber generating (FG) mode, while filament extrusion (FE) works when the nozzle is out. The opening distance between the air knife module and the heated block was chosen as a minimum of 1 mm for smooth operating.

A Velleman K8200 desktop FFF printer (Velleman vn, Belgium) used to test the developed apparatus. Two K-type thermocouples, one mounted to an air knife module (7) and the other mounted to a heated block (8), and a PID control unit was used to heat up and control the apparatus temperature. The apparatus temperature was set to a constant 200 °C. The air temperature was heated by an inline heater (AHPF-082, Omega, UK) and the air temperature was measured in line with a K-type inline nozzle thermocouple. The hot air temperature was set to 250 °C and held constant with a PID controlling unit. The zero distance between the apparatus and the printing plate was set with paper (50 μm). I used open-source Printrun 2.X software (Pronterface, GNU General Public License) for controlling the FFF printer via computer.

The distance between the apparatus and the printing bed was set constant at 100 mm for fiber generating. The filament drawing speed was set to 1 mm/min. The nozzle diameter of 0.2, 0.4 and 0.5 mm were tested. The influence of three air pressure levels (1, 1.5 and 2 bar) and two air knife angles (35°and 60°) on the fiber properties were tested.

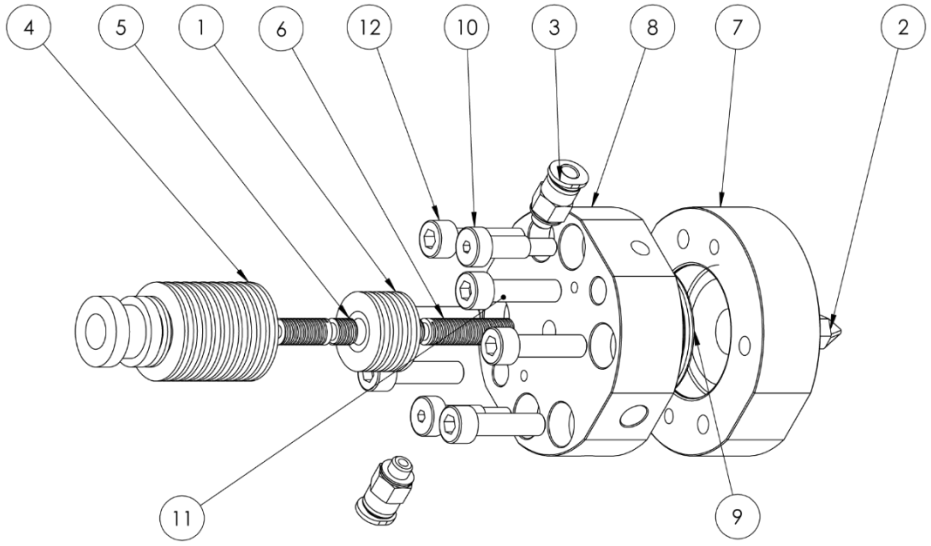

Figure 3. Exploded view of the developed FFF apparatus; 1: heat sink, 2: nozzle, 3: air tube connector, 4: heat sink, 5: throat heat break, 6: throat heat break, 7: air knife module, 8: heated block, 9: O-ring, 10: shoulder bolt (leveling), 11: bolt (leveling), 12: bolt (joining)

A PLLA homopolymer resin was used to prepare filaments for FFF 3D printing. I used PLLA filament to generate fibers and 3D print structures. PLLA filaments (filament diameter 1.75 mm) were produced with a Precision 450 type filament maker (3devo B.V., Netherland). The temperature profile was set to 185-210-195-185 °C (from hopper to die). The extruder screw rotation speed was set to 2.4 rpm.

I investigated the accuracy between the CAD model and printed parts. I used SolidWorks 16 (Dassault Systèmes, France) to design the 3D model sample with dimensions of 80 x 10 x 1.5 [mm] (length x width x thickness). The apparatus and printing bed temperature were set to 200 °C and 60 °C, respectively. The nozzle diameter and filament drawing speed were 0.2 mm and 60 mm/s, respectively. The 3D printed samples were compared in terms of geometry and precision with the 3D CAD model. I produced 5 samples. I measured the 3D printed sample's length, thickness and width using a digital caliper (Fowler Promax, USA).

4.10.1. Ansys airflow field simulations

One-quarter of the whole geometry was modeled using symmetry simplification to reduce the computational cost. The structured mesh had hexahedra elements in the inflation layer near the wall and tetrahedra cells inside the flow domain. The inflation layer was 0.2 mm in width and contained 5 layers with a growth rate of 1.2. The mesh is refined inside the apparatus and in the vicinity of the apparatus orifice.

To eliminate the discretization error, mesh independence analysis was performed with three different mesh sizes. I tested 1456k, 2998k, and 6782k elements for the air knife with a half-cone opening angle of 60°, and the obtained air flow rate values compared to the measurement data. The results show that the relative difference in the obtained values was less than 1% in the case of the three meshes. Considering simulation time and the difference between the simulation and experimental data, the mesh with 2998k cells was chosen for the simulations.

The heated and pressurized air flows inside the apparatus at the inlet described with a p_{in} relative pressure and T_{in} temperature. It is assumed that there is only a short time for heat exchange due to the high velocities; therefore, the heat transfer inside the nozzle was neglected. The apparatus inside walls were modeled with adiabatic no-slip walls. On the other hand, the outer wall temperature was set to 20 °C, according to the empirical observations.

The environment was represented by the opening boundary condition with $T_{env} = 20°C$ temperature and $p_{env} = 0$ Pa entrainment pressure. The fiber collector plane was considered with a 20 °C, no-slip wall.

For validation purposes, two independent cases were considered. In the first case, the volume flow rate was calculated when the inlet temperature was equal to ambient, $T_{in} = T_{env} = 20°C$, and the pressure varies between 0.4-2.4 bars. In that case, the outer wall of the apparatus was $T_{wall} = 20°C$. In the second case, the temperature distribution was determined when $T_{in} = 250°C$ and $p_{in} = 1$ bar. For that, the outer apparatus wall temperature was $T_{wall} = 200$ °C. Furthermore, the previous two cases were combined to validate those experimental observations, i.e., the $p_{in} = 1; 1.5; 2$ bar, $T_{in} = 250°C$, and $T_{wall} = 200$ °C.

The air was considered to be an ideal gas with $\mu = 1.831 \cdot 10^{-5}$ Pas dynamic viscosity, $\lambda = 0.0261$ W/(mK) thermal conductivity and $c_p = 1004.4$ J/(kg K) specific heat (at constant pressure) at 25 °C reference temperature. Because the computational domain contains narrow (inside the apparatus) and large far-field (outside the apparatus) regions, the *Shear Stress Transport* (SST) turbulence model was applied with an automatic wall function. As a result, a set of equations for the continuity, energy, momentum, turbulent eddy frequency and turbulence kinetic energy were solved.

Since the real application is time-independent, steady-state simulations were performed with high-resolution advection and first-order turbulence schemes. The convergence criteria were set to 10^{-5}, while the volume flow rate was monitored. The simulation stopped when the convergence criteria and the steady-state solution of the volume flow rate were reached.

4.11.1. Air temperature and flow rate measurement

To verify the airflow field CFD model, I measured and predicted the effects of air knife design and air pressure on velocity and temperature distributions. I conducted experiments to measure airflow rate at the apparatus inlet and air temperature after air exits the apparatus. I measured the temperature inline with a K-type bare thermocouple and a digital thermometer (Testo 830-T2, Germany). The thermocouple was placed parallel to the tool to read the air centerline temperature. With this aim, the thermocouple was set and fixed to variable distances (5-40 mm) from the apparatus during the experiments. The temperature was recorded when the read value reached a stable region, *e.g.*, ±1 °C. A digital airflow meter (flow switch, PFMB721-C8-F, SMC, Japan) was used to measure the air volume flow rate. I measured the air volume flow rate without heating it at room temperature. The air pressures in the range of 0.4-2.4 bar were applied, and the corresponding flow rates were recorded. I recorded the volume flow rate corresponding to the standard condition (T = 15 °C, p = 101.3 kPa), where the density is $\rho_{airstd} = 1.225 \frac{kg}{m^3}$.

5. Theses

1. I proved that in the case of melt-blown polypropylene fiber mats, there is a relationship between the self-bonding quality & tensile strength and structural parameters. I introduced the mat consolidation coefficient (MCC) that describes this:

$$MCC = \frac{S \times \mathrm{d}_{f,m}}{DP_m} \; [-]$$

where S is the solidity, $d_{f,m}$ is the average fiber diameter and DP_m is the average pore size. The higher the MCC the higher the tensile strength and the stronger the bonds between the fibers. The MCC ($0 < MCC \leq 1$) effectively describes the fiber mat characteristics in the parameter range of $50\,mm \leq die\ to\ collector\ distance \leq 500\,mm$, $125\,°C \leq air\ temperature \leq 300\,°C$ and $1\,bar \leq air\ pressure \leq 2.5\,bar$. MCC can be effectively used to characterize the mat's

characteristics if $0.01 < d_{f,m}/DP_m < 2$ and $0.05 < S < 0.5$. I showed that the MCC and the tensile strength had a good linear relation (R^2=0.95), where MCC was in the range of 0.07-0.27. [P9-P10]

2. I proved that hot-compacted single-polymer composites made of melt-blown fine fiber mats had higher specific strength by up to 109%. I proved via differential scanning calorimetry that the degree of crystallinity of these composites was higher by up to 16% (from 54 to 63 percentage points) than that of the pristine fiber mat, revealing that fine fibers created nucleation sites in the matrix. Scanning electron microscopy revealed that the composite had a fair consolidation and low void content, and besides, the fibers kept their structural integrity during the composite processing. [P8, P11]

3. I proved the applicability of fine fiber interleaving in single-polypropylene composites, where the interleaves are made of the same polymer. This interleaving improved the interlaminar shear strength by 17%, the tensile modulus by 46%, and the falling dart perforation energy by up to 26%. I showed that the storage modulus significantly increased while the tanδ decreased. With the aid of scanning electron microscopy, I proved that the melt-blown fiber interleaves created a net-like structure leading to enhanced interfacial strength that caused the improvement at a macroscopic level. I demonstrated via differential scanning calorimetry that the interleaves acted as a nucleating agent at the matrix interface, translating to an enhanced degree of crystallinity (by up to 6 percentage points higher). [P11-P12]

4. I embedded multiwalled carbon nanotubes into polypropylene melt-blown fibers and those enhanced the fiber mats' mechanical and thermal properties. The specific strength, peak crystallization temperature and onset thermal decomposition temperature were increased by 78%, 7 °C and up to 77 °C, respectively. The improvement was due to the presence of carbon nanotubes and the nucleation sites created along them, which is confirmed by differential scanning calorimetry. I revealed that interleaving single-polypropylene composites with polypropylene mats enhanced their thermal and mechanical properties. The presence of carbon nanotubes embedded into the fibers further improved these properties. The tensile modulus increased by up to 37% and the storage modulus by 33%, while the tanδ decreased by around 10%. With the aid of digital image correlation, I showed that the interleaved laminate had the lowest local strains at the tensile test. I proved that this enhanced damage tolerance and stiffness originates from the advanced properties of the fiber mat. [P13]

5.a I demonstrated the applicability of melt blowing to produce poly(lactic acid) fine fibers from various PLLA and PDLA enantiomer blends with stereocomplex and homocrystalline structures. Generating melt-blown fibers with stereocomplex crystals (1:1, PLLA:PDLA) decreased the average fiber diameter by 80% and resulted in up to 60% higher specific strength than those of the pristine PLLA and PDLA fiber mats. With the aid of differential scanning calorimetry, I proved that melt blowing enhances the stereocomplex crystal formation by shear-induced crystallization, which led to these improvements.

5.b I revealed that poly(lactic acid) melt-blown fine fiber mat samples subjected to composting soil and warm water showed a fast decomposition. I concluded that the fast decomposition was due to the high porosity and high surface area of the fiber mats. I proved that the samples decomposed and extensively disintegrated in 70 days in water and in less than 40 days in compost. With the aid of scanning electron microscopy, I revealed that hydrolysis resulted in surface and bulk erosion in general, while the stereocomplex-crystalline-rich domains primarily exhibited surface erosion. I proved that stereocomplexation did not hinder the decomposition of melt-blown fiber mats in compost and in water. [P14]

6. I invented a novel 3D printing apparatus to generate hierarchical structures consisting of *in-situ* melt-blown fiber mats and fused filament fabrication printed struts. I showed that the novel apparatus could generate poly(lactic acid) fibers as small as 300 nm using a conventional 3D printing filament as feedstock material. I demonstrated that the novel apparatus could successfully generate objects by adding material based on a geometrical representation given by a CAD model. I analyzed the airflow field and proved that the air knife angle (35° *vs.* 60°) greatly influences the fiber mat properties. With the aid of computational fluid dynamics simulation, I demonstrated that the air reaches supersonic velocities during operation. The 60° air knife angle resulted in 7-12% thinner fibers and a two-fold increase in the specific strength at the same applied air pressure. With the aid of differential scanning calorimetry, I proved that the fibers' glass transition temperature and crystallinity are 4 °C and 6 percentage points higher, respectively, than those of the filament. That is an advantage in keeping the structural integrity of the fibers when the 3D printer adds the next layer of dispensed molten material during the process. [P15]

6. Publications and patents

P1. **Yahya Kara**, Hamit Akbulut, *Helical Springs Made of Polymer Nanocomposite: Optimization for Design Variables of Carbon Fiber Reinforced Carbon Nanotube Additive Epoxy Composites*, Lambert Academic Publishing (LAP), Germany, ISBN: 978-3-659-92120-9, (2016)

P2. **Yahya Kara**, Hamit Akbulut, *Mechanical Behavior of Helical Springs Made of Carbon Nanotube Additive Epoxy Composite Reinforced with Carbon Fiber*, Journal of the Faculty of Engineering and Architecture of Gazi University, 32(2), 417–427, (2017), https://doi.org/10.17341/gazimmfd.322166

P3. **Yahya Kara**, *A Review: Fiber Reinforced Polymer Composite Helical Springs*, Journal of Materials Science & Nanotechnology (5)1, 101-107, (2017), https://doi.org/10.15744/2348-9812.5.101

P4. Haijun He, **Yahya Kara**, Kolos Molnár, *Effect of needle characteristic on fibrous PEO produced by electrospinning*, Resolution and Discovery, 4(1), 7–11, (2019), https://doi.org/10.1556/2051.2018.00063

P5. Haijun He, **Yahya Kara**, Kolos Molnár, *In situ viscosity controlled electrospinning method: The effect of gap size on nanofiber morphology*, Macromolecular Materials and Engineering, 304(11), 1900349, (10 pages), (2019), https://doi.org/10.1002/mame.201900349

P6. **Yahya Kara**, Haijun He, Kolos Molnár, *Shear-Aided High-Speed Electrospinning: A Needleless Method with Enhanced Jet Formation*, Journal of Applied Polymer Science, 137(37), (13 pages), (2020), https://doi.org/10.1002/app.49104

P7. László Mészáros, **Yahya Kara**, Tamás Fekete, Kolos Molnár, *Development of self-reinforced low-density polyethylene using γ-irradiation cross-linked polyethylene fibres,* Radiation Physics and Chemistry, 170, 108655, (6 pages), (2020), https://doi.org/10.1016/j.radphyschem.2019.108655

P8. Ábris Dávid Virág, **Yahya Kara**, László Mihály Vas, Kolos Molnár, *Single Polymer Composites Made of Melt-blown PP Mats and the Modelling of the Uniaxial Tensile Behaviour by the Fibre Bundle Cells Method*. Fibers and Polymers, 22, 2700–2713, (2021) https://doi.org/10.1007/s12221-021-0038-6

P9. **Yahya Kara**, Kolos Molnár, *Revealing of process-structure-property relationships of fine PP fiber mats generated via melt blowing*, Polymers for Advanced Technologies, 32(6), 2416– 2432 (2021), https://doi.org/10.1002/pat.5270

P10. **Yahya Kara**, Kolos Molnár, *A review of processing strategies to generate melt-blown nano/microfiber mats for high-efficiency filtration applications*. Journal of Industrial Textiles, 51, 137S-180S, (2021) https://doi.org/10.1177/15280837211019488

P11. **Yahya Kara**, Kolos Molnár, *Melt-blown fiber mat interleaving enhances the performance of single-Polypropylene composites, Journal of Reinforced Plastics and Composites, (12 pages), (2022),* https://doi.org/10.1177/07316844221087736

P12. **Yahya Kara**, Kolos Molnár, *Development of Polypropylene Melt-Blown Fine Fiber Interleaved Single-Polypropylene Composites*, Composites Meet Sustainability – Proceedings of the 20th European Conference on Composite Materials, ECCM20. 26-30 June, 2022, Lausanne, Switzerland

P13. **Yahya Kara**, Kolos Molnár, *Development of single-polypropylene composites interleaved with MWCNT doped melt-blown fine fiber mats*, Polymer Composites, 43(8), 5208, (10 pages), (2022), https://doi.org/10.1002/pc.26812

P14. **Yahya Kara**, Kolos Molnár, *Decomposition behavior of stereocomplex PLA melt-blown fine fiber mats in water and compost, Journal of Polymers and the Environment,* ***under review***

P15. **Yahya Kara**, Norbert Krisztián Kovács, Kolos Molnár, *An apparatus for a fiber-forming 3D printer, a 3D printer incorporating such an apparatus, and a method of making a 3D printed polymer composite* (Nyomtatófej szálhúzásos 3D nyomtatóhoz, 3D nyomtató, amely ilyen nyomtatófejet tartalmaz, valamint eljárás 3D nyomtatott polimer kompozit előállítására), Patent filed, P2200146, Hungary (09.05.2022)

P16. Kolos Molnár, Haijun He, Bálint Budavári, Krisztina S. Nagy, Angéla Jedlovszky-Hajdú, **Yahya Kara**, *Nano-hydroxyapatite reinforced, 3D printed photopolymer-based composites for biomedical applications*, Composites Meet Sustainability – Proceedings of the 20th European Conference on Composite Materials, ECCM20. 26-30 June, 2022, Lausanne, Switzerland.

P17. **Yahya Kara,** Volkan Acar, M. Özgür Seydibeyoğlu, *Mechanical properties of nanoparticle-based polymer composites*, In Nanoparticle-Based Polymer Composites, Eds: Sanjay M.R., Jyotishkumar P., Yashas T.G., Suchart S., Seydibeyoglu M. O., Elsevier Woodhead Publishing Series in Composites Science and Engineering, 95-108, (2022), https://doi.org/10.1016/B978-0-12-824272-8.00007-5